

Considerations on the suppression of charged particles and π^0 in high energy heavy ion collisions

M.Petrovici,^{1,2} A.Lindner,^{1,2} and A.Pop¹

¹*National Institute for Physics and Nuclear Engineering - IFIN-HH
Hadron Physics Department
Bucharest - Romania*

²*Faculty of Physics, University of Bucharest
(Dated: February 3, 2021)*

Experimental results related to charged particle and π^0 suppression obtained at the Relativistic Heavy Ion Collider (RHIC) at Brookhaven for Au-Au (Cu-Cu) collisions and at the Large Hadron Collider (LHC) at CERN for Pb-Pb (Xe-Xe) collisions are compiled in terms of the usual nuclear modification factors, R_{AA} and R_{CP} , and of the newly introduced R_{AA}^N and R_{CP}^N as a function of $\langle N_{part} \rangle$ and $\langle dN_{ch}/d\eta \rangle$. The R_{AA}^N and R_{CP}^N are calculated as the ratios of the p_T spectra in each centrality bin, to the spectrum in proton-proton minimum bias collisions, or to the spectrum in a peripheral bin, respectively, each of them normalised to the corresponding charged particle density. The studies are focused on a p_T range in the region of maximum suppression evidenced in the experiments. The R_{AA} scaling as a function of $\langle N_{part} \rangle$ and $\langle dN_{ch}/d\eta \rangle$ is discussed. The core contribution to R_{AA} is presented. The difference in R_{AA} relative to the difference in particle density per unit of rapidity and unit of overlapping area ($\langle dN/dy \rangle / S_{\perp}$) and the Bjorken energy density times the interaction time ($\varepsilon_{Bj} \cdot \tau$) between top RHIC and LHC energies indicate a suppression saturation at LHC energies. Considerations on the missing suppression in high charged particle multiplicity events for pp collisions at 7 TeV are presented. R_{CP}^N for the same systems and energies shows a linear scaling as a function of $\langle N_{part} \rangle$. While $(1-R_{AA})/\langle dN/dy \rangle$ shows an exponential decrease with $(\langle dN/dy \rangle / S_{\perp})^{1/3}$, $(1-R_{AA}^N)/\langle dN/dy \rangle$ is independent on $(\langle dN/dy \rangle / S_{\perp})^{1/3}$ for $(\langle dN/dy \rangle / S_{\perp})^{1/3} \geq 2.1$ particles/ $fm^2/3$. The trends of R_{CP} and R_{CP}^N for charged particles as a function of $\sqrt{s_{NN}}$, measured at RHIC in Au-Au collisions and at LHC in Pb-Pb collisions, show a suppression that becomes larger from $\sqrt{s_{NN}} = 39$ GeV up to $\sqrt{s_{NN}} = 200$ GeV, followed by a saturation up to the highest energy of $\sqrt{s_{NN}} = 5.02$ TeV in Pb-Pb collisions. The $\sqrt{s_{NN}}$ dependences of $R_{AA}^{\pi^0}$ and $(R_{AA}^N)^{\pi^0}$ in the same p_T ranges and for the very central collisions show the same trend. A clear change in the dependence of $(1 - R_{AA}^{\pi^0})/\langle dN/dy \rangle$ for the most central collisions as a function of collision energy is evidenced in the region of $\sqrt{s_{NN}} = 62.4 - 130$ GeV.

I. INTRODUCTION

Detailed studies of different observables in heavy ion collisions at RHIC [1–6] support theoretical predictions pioneered more than 40 years ago [7–10] that at large densities and temperatures of the fireballs produced at these energies, the matter is deconfined into its basic constituents, quarks and gluons. Obviously, such studies are rather difficult given that the produced fireballs are highly non-homogeneous, have a small size and are highly unstable, since their dynamical evolution plays an important role. One of the powerful tools used to diagnose the properties of such a deconfined object is the study of the energy loss of partons traversing the deconfined matter [11]. Within QCD based models, the energy loss of a parton traversing deconfined matter is due to collisional or radiative processes. Collisional energy loss due to elastic parton collisions is expected to scale linearly with the path length [12]. Radiative energy loss occurs via inelastic processes where a hard parton radiates a gluon. Soft interactions of partons with the deconfined medium can also induce gluon radiation [13]. Radiative energy loss is expected to grow quadratically with the path length [14]. There are quite a few theoretical approaches to describe the parton energy loss in expanding

deconfined matter [15–24]. However, a proper description of the parton energy loss in the non-equilibrium expanding deconfined matter for the intermediate p_T range remains a challenging task. The predicted suppression at LHC energies turned out to be overestimated, once the experimental information became available. A comprehensive analysis within the CUJET/CIBJET framework recently published [25], indicates, similar to the results of the JET Collaboration [22], a maximum in \hat{q}/T^3 as a function of temperature around the critical temperature (T_c), followed by a decrease towards temperatures reached at LHC energies. Some considerations on the charged particle and π^0 suppression at RHIC and LHC energies are presented in this paper. Section II is a short presentation of the quantities estimated in the Glauber Monte Carlo (MC) model used in the next sections. A review of the charged particle suppression dependence on $\langle N_{part} \rangle$ and $\langle dN_{ch}/d\eta \rangle$, the core-corona effect and the dependence on particle density per unit of rapidity and unit of overlapping area ($\langle dN/dy \rangle / S_{\perp}$), a measure of the entropy density and thus of temperature [26] and the Bjorken energy density times the interaction time ($\varepsilon_{Bj} \cdot \tau$) for Cu-Cu and Au-Au at the top RHIC energy and for Xe-Xe and Pb-Pb at LHC energies, are presented in Section III. Section IV is dedicated

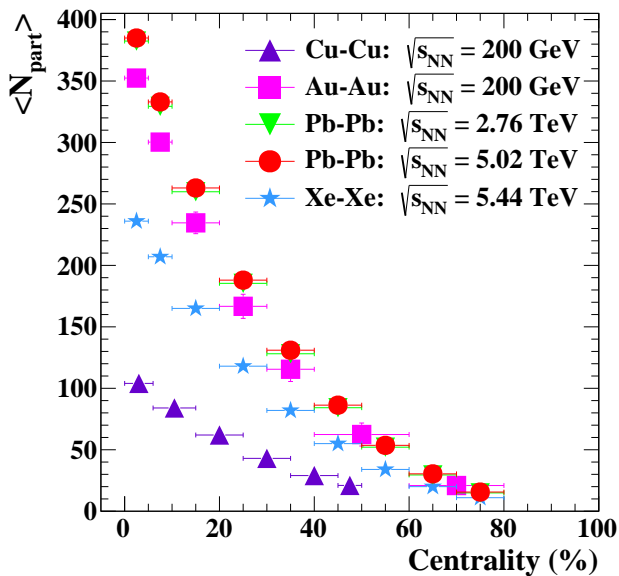


FIG. 1. The average number of participating nucleons $\langle N_{part} \rangle$ as a function of centrality for Cu-Cu, Au-Au collisions at $\sqrt{s_{NN}} = 200$ GeV, for Xe-Xe at $\sqrt{s_{NN}} = 5.44$ TeV and for Pb-Pb at $\sqrt{s_{NN}} = 2.76$ and 5.02 TeV.

to similar studies, using $\langle dN_{ch}/d\eta \rangle^{AA}/\langle dN_{ch}/d\eta \rangle^{pp}$ instead of $\langle N_{bin} \rangle$ in a model independent estimation of suppression, namely R_{AA}^N , defined later in this section [27]. In Section V, similar considerations for the corresponding relative suppression, R_{CP} and R_{CP}^N are presented. $(1-R_{AA})/\langle dN/dy \rangle$ and $(1-R_{AA}^N)/\langle dN/dy \rangle$ dependences as a function of $(\langle dN/dy \rangle/S_{\perp})^{1/3}$ are presented in Section VI. The collision energy dependence of R_{CP} , R_{CP}^N for charged particles and R_{AA} , R_{AA}^N for π^0 is discussed in Section VII. Conclusions are presented in Section VIII.

II. GLAUBER MONTE CARLO ESTIMATES

The Glauber MC model [28–31] was used to estimate in a unitary manner various quantities characteristic to the initial state in A-A collisions: number of participants, number of collisions, number of nucleons undergoing a single collision and the transverse overlapping areas in centrality bins. In a core-corona picture [31], the core quantities were estimated for wounded nucleons suffering more than a single collision. The calculations have been done in the hard sphere wounding prescription [31]. For the nuclear density profile of the colliding nuclei, a Woods-Saxon distribution was considered:

$$\rho(r) = \frac{1}{1 + \exp(\frac{r-r_0}{a})} \quad (1)$$

with $a = 0.535$ fm, $r_0 = 6.5$ fm for the Au nucleus [32], $a = 0.546$ fm, $r_0 = 6.62$ fm for the Pb nucleus [76] $a = 0.57$ fm, $r_0 = 5.42$ fm for the Xe nucleus [34] and $a = 0.596$ fm, $r_0 = 4.2$ fm for the Cu nucleus [34]. Within

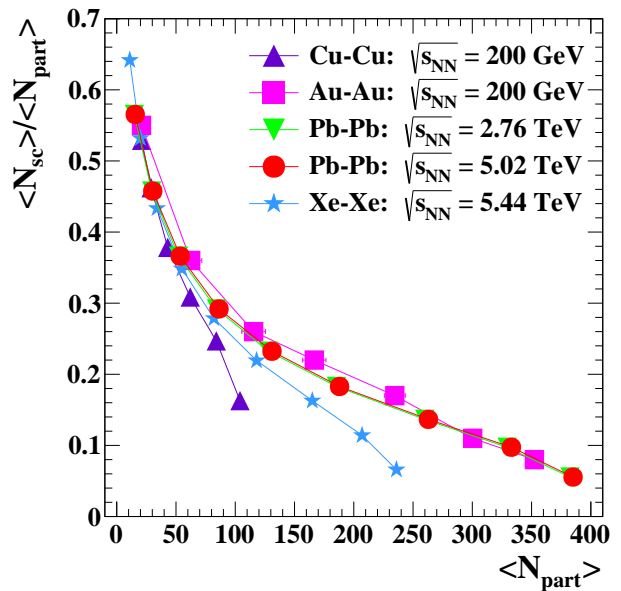


FIG. 2. Ratio of the average number of nucleons undergoing single collisions to the average number of participating nucleons ($\langle N_{sc} \rangle / \langle N_{part} \rangle$), as a function of the average number of participating nucleons ($\langle N_{part} \rangle$) estimated within the Glauber MC model.

the hard sphere approach, the nucleons are considered to collide if the relative transverse distance $d \leq \sqrt{\frac{\sigma_{pp}}{\pi}}$. The nucleon - nucleon inelastic cross section, σ_{pp} , at a given collision energy, was taken as specified in Refs. [32, 36, 42, 76]. The centrality dependence of the overlapping area, S_{\perp}^{var} is considered to be proportional to the quantity $S \propto \sqrt{\langle \sigma_x^2 \rangle \langle \sigma_y^2 \rangle - \langle \sigma_{xy}^2 \rangle}$. σ_x^2 , σ_y^2 are the variances, and σ_{xy} is the co-variance of the participant distributions in the transverse plane, per event [37]. They were averaged over many events. The centrality dependent values were rescaled in such a way as to equalize the geometrical area (calculated as in [38, 39]) and S_{\perp}^{var} in the case of the complete overlap of the nuclei ($b = 0$ fm). After generating a large number of events for the minimum bias (MB) collisions, they were sorted in centrality classes according to the impact parameter distribution. Calculations of the quantities of interest have been done in each centrality class. The results of the calculations for various systems and energies were presented in Refs. [38, 39] and Table I of this paper. The obtained number of participants and number of collisions are in good agreement, within the error bars, with the same quantities listed in different experimental publications. In Figure 1, the average number of participating nucleons ($\langle N_{part} \rangle$) [35, 36, 38, 40, 41] as a function of centrality obtained within the Glauber MC approach is shown. As can be seen, the difference in $\langle N_{part} \rangle$ at a given centrality, for colliding systems with different sizes and incident energies, is increasing from peripheral towards central collisions. Figure 2 shows the average number of nucleons un-

dergoing single collisions relative to the average number of participating nucleons ($\langle N_{sc} \rangle / \langle N_{part} \rangle$). As expected, $\langle N_{sc} \rangle / \langle N_{part} \rangle$ has large values at low $\langle N_{part} \rangle$, the system size and collision energy dependence being rather small. With increasing $\langle N_{part} \rangle$ towards very central collisions, although the percentage of nucleons undergoing single collisions decreases, the difference between the various systems becomes significant.

TABLE I: The percentage of nucleons that suffer more than a single collision (f_{core}), the overlapping surface of the colliding nuclei (S_{\perp}^{var}) and the overlapping surface corresponding to the core contribution ($(S_{\perp}^{var})^{core}$) for Cu-Cu and Xe-Xe colliding systems at the corresponding collision energies and centralities.

System	$\sqrt{s_{NN}}$ (GeV)	Cen. (%)	f_{core}	S_{\perp}^{var} (fm^2)	$(S_{\perp}^{var})^{core}$ (fm^2)
Cu-Cu	200	0-10	0.81 ± 0.00	67.9 ± 0.5	51.8 ± 0.4
		10-30	0.69 ± 0.00	53.4 ± 0.4	36.1 ± 0.3
		30-50	0.55 ± 0.00	38.3 ± 0.3	23.3 ± 0.2
		50-70	0.38 ± 0.01	24.7 ± 0.2	13.2 ± 0.1
Xe-Xe	5440	0-5	0.93 ± 0.00	124.1 ± 0.6	105.3 ± 0.5
		5-10	0.89 ± 0.00	114.9 ± 0.6	91.3 ± 0.5
		10-20	0.84 ± 0.00	100.6 ± 0.5	74.9 ± 0.4
		20-30	0.78 ± 0.00	83.7 ± 0.5	57.9 ± 0.3
		30-40	0.72 ± 0.00	69.3 ± 0.4	44.7 ± 0.2
		40-50	0.65 ± 0.00	57.1 ± 0.3	34.2 ± 0.2
		50-60	0.57 ± 0.00	45.9 ± 0.3	25.5 ± 0.1
		60-70	0.47 ± 0.01	35.4 ± 0.2	18.2 ± 0.1
70-80	0.36 ± 0.01	24.8 ± 0.2	10.9 ± 0.1		

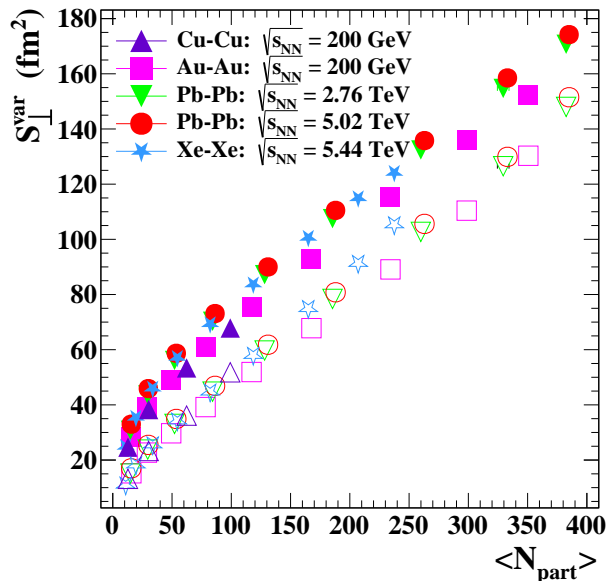


FIG. 3. The overlapping area (S_{\perp}^{var}) as a function of $\langle N_{part} \rangle$ corresponding to total (full symbols) and core (open symbols) wounded nucleons.

Figure 3 shows the overlapping area, S_{\perp}^{var} , as a function of $\langle N_{part} \rangle$ for the total and core contribution. In this paper we decided to use S_{\perp}^{var} , similar to what was used

to estimate the Bjorken energy density at LHC energies [43]. It will be simply written S_{\perp} from now on.

III. R_{AA} ($5 < p_T < 8$ GeV/c) : $\langle N_{part} \rangle$ DEPENDENCE

Usually, the comparisons among different systems and different collision energies in terms of the nuclear modification factor, R_{AA} , are done as a function of collision centrality. R_{AA} is defined as:

$$R_{AA} = \frac{(\frac{d^2N}{d\eta dp_T})^{cen}}{\langle N_{bin} \rangle \cdot (\frac{d^2N}{d\eta dp_T})^{pp,MB}} \quad (2)$$

where the transverse momentum distribution of a certain particle measured in A-A collisions for a given centrality (cen) is divided by the pp MB p_T distribution of that particle at the same energy, multiplied by the number of binary collisions calculated based on the Glauber MC model. Because of the $\langle N_{part} \rangle$ dependence on centrality in Figure 1, a study of the suppression phenomena in relativistic heavy ion collisions as a function of system size and collision energy is better done in terms of $\langle N_{part} \rangle$, instead of centrality. At $\sqrt{s_{NN}}=200$ GeV, the same values of charged particle R_{AA} as a function of $\langle N_{part} \rangle$ for different bins in p_T , for two very different colliding symmetric systems Au-Au [44] and Cu-Cu [40], were evidenced. A similar scaling was also observed for a lower collision energy, i.e. $\sqrt{s_{NN}}=62.4$ GeV [45]. Such a dependence was studied for pions and protons, for $5 < p_T < 8$ GeV/c and $5 < p_T < 6$ GeV/c respectively, in Cu-Cu and Au-Au collisions at $\sqrt{s_{NN}}=200$ GeV, by the STAR Collaboration [46], where a good scaling of $R_{AA}^{\pi^+\pi^-}$ as a function of $\langle N_{part} \rangle$ for the two systems was seen. The PHENIX Collaboration has shown that in Au-Au collisions at $\sqrt{s_{NN}}=62.4$ GeV and 200 GeV, the R_{AA} of π^0 for $p_T > 6$ GeV/c has the same value as a function of $\langle N_{part} \rangle$ [47]. At the LHC energies, the CMS Collaboration presented a similar scaling for Xe-Xe at $\sqrt{s_{NN}}=5.44$ TeV and Pb-Pb at $\sqrt{s_{NN}}=5.02$ TeV [48] with the remark that the R_{AA} for Xe-Xe was obtained using the p_T spectrum from MB pp collisions at $\sqrt{s}=5.02$ TeV. Aside from Cu-Cu at $\sqrt{s_{NN}}=200$ GeV, where the p_T spectra were obtained for the $0.2 < \eta < 1.4$ pseudorapidity range, all the other results were obtained for a symmetric cut relative to $\eta=0$.

Suppression studies at LHC energies up to very large p_T values [49–51], for charged particles, evidence a maximum suppression in the 5-8 GeV/c p_T range, for a given centrality. While the absolute value of the maximum suppression depends on centrality, its position is in the same region of p_T . Although at RHIC energies the measured p_T range is much smaller than the region where the R_{AA} starts to increase, based on the larger range in p_T for π^0 [47], one could conclude that the maximum suppression for different centralities is in the same range of p_T , i.e.

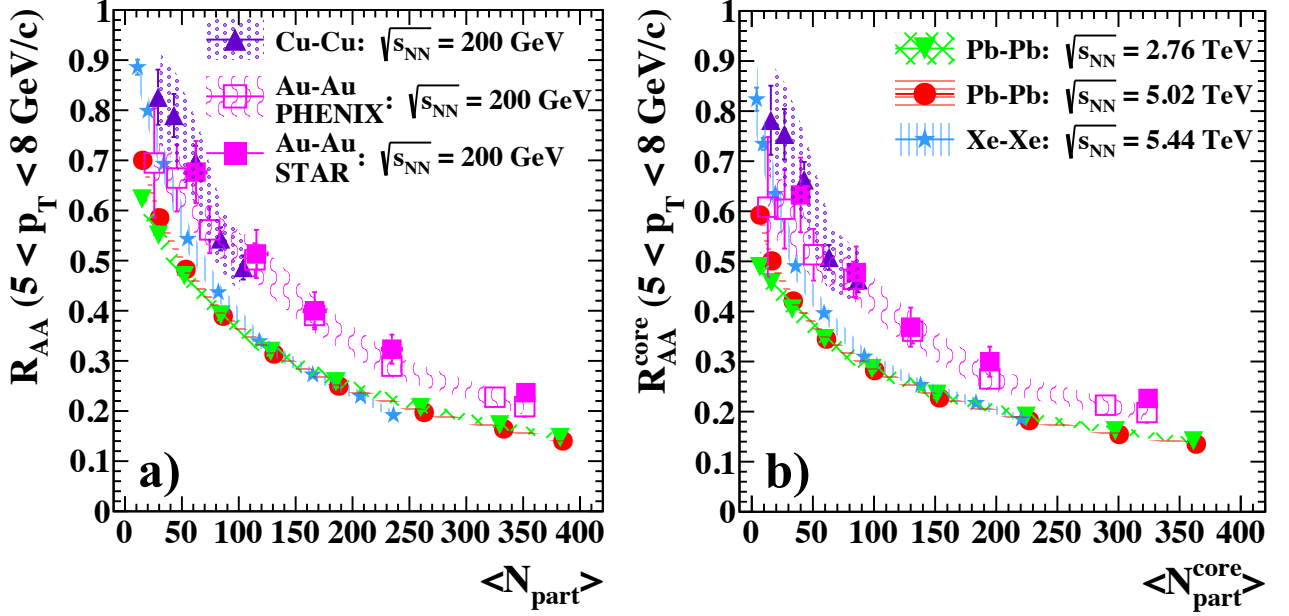


FIG. 4. R_{AA} in the $5 < p_T < 8$ GeV/c region as a function of the average number of nucleons $\langle N_{part} \rangle$ for charged particles; a) experimental values, b) core contribution, see the text.

5-8 GeV/c. This is the main reason to focus the present considerations on the suppression phenomena in this p_T range.

Using the latest results obtained at RHIC for Cu-Cu and Au-Au collisions at $\sqrt{s_{NN}}=200$ GeV [40, 41, 44], at LHC for Xe-Xe at $\sqrt{s_{NN}}=5.44$ TeV [35] and Pb-Pb at $\sqrt{s_{NN}}=2.76$ and 5.02 TeV [52], we obtained the mean values of R_{AA} , averaged over the $5 < p_T < 8$ GeV/c region, presented in Figure 4a. R_{AA} scales as a function of $\langle N_{part} \rangle$ at RHIC ($\sqrt{s_{NN}}=200$ GeV) and LHC energies, separately, as it was shown in the above mentioned papers. Within the error bars, a small difference, i.e. a slightly larger suppression is observed for central Cu-Cu and Xe-Xe collisions relative to Au-Au and Pb-Pb respectively, at the same $\langle N_{part} \rangle$. The highlighted areas represent the systematic uncertainties, while the error bars are the statistical uncertainties, for the cases where they have been reported separately (Pb-Pb at $\sqrt{s_{NN}}=2.76$ and 5.02 TeV, Xe-Xe at $\sqrt{s_{NN}}=5.44$ TeV, Au-Au (PHENIX) and Cu-Cu at $\sqrt{s_{NN}}=200$ GeV), while in the case of Au-Au (STAR) the error bars represent the square root of statistical and systematic uncertainties added in quadrature. Another aspect worth being considered is the so called core-corona effect [53–64] on the suppression estimate. The contribution to the p_T spectra in A-A collisions from a nucleon suffering a single collision is similar with the spectra from pp MB collisions at the same energy. Therefore, one should first correct the experimental spectra of A-A collisions with the contribution coming from single binary collisions (corona) in order to obtain the spectra

of the core:

$$\begin{aligned} \left(\frac{d^2N}{d\eta dp_T}\right)^{cen,core} &= \left(\frac{d^2N}{d\eta dp_T}\right)^{cen,measured} - \\ &- \left(\frac{d^2N}{d\eta dp_T}\right)^{pp,MB,measured} \cdot \frac{\langle N_{part} \rangle^{cen}}{2} \cdot (1 - f_{core}^{cen}), \end{aligned} \quad (3)$$

where $f_{core}^{cen} = \langle N_{part}^{core} \rangle^{cen} / \langle N_{part} \rangle^{cen}$. The suppression due to the core of the fireball, R_{AA}^{core} :

$$R_{AA}^{core} = \frac{\left(\frac{d^2N}{d\eta dp_T}\right)^{cen,core}}{\langle N_{bin}^{core} \rangle^{cen} \cdot \left(\frac{d^2N}{d\eta dp_T}\right)^{pp,MB}}, \quad (4)$$

where

$$\langle N_{bin}^{core} \rangle^{cen} = \langle N_{bin} \rangle^{cen} - \frac{\langle N_{part} \rangle^{cen}}{2} \cdot (1 - f_{core}^{cen}) \quad (5)$$

is presented in Figure 4b as a function of $\langle N_{part}^{core} \rangle$. In the simple image of a net core-corona separation, the figure shows the core contribution extracted from the experimental data for the different centrality classes.

The suppression is increased in peripheral collisions by ≈ 10 -20% and the values for the most central Cu-Cu and Xe-Xe collisions are the same as for Au-Au and Pb-Pb collisions, respectively, for the same $\langle N_{part} \rangle$. The suppression for Cu-Cu and Au-Au is the same at the same collision energy ($\sqrt{s_{NN}}=200$ GeV). At the LHC energies, the suppression in Pb-Pb collisions at $\sqrt{s_{NN}}=2.76$ TeV is the same as at $\sqrt{s_{NN}}=5.02$ TeV, as well as for Xe-Xe at $\sqrt{s_{NN}}=5.44$ TeV, where the latter energies are almost twice as high. The small deviation evidenced in Xe-Xe

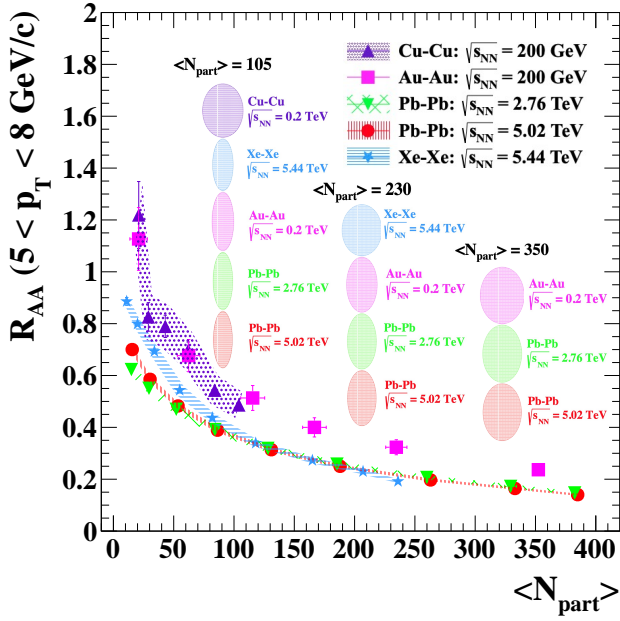


FIG. 5. The same as Figure 4a with the shape of the overlapping area S_{\perp} at different values of $\langle N_{part} \rangle$ estimated within the Glauber MC approach.

collisions at low values of $\langle N_{part} \rangle$ could be due to the way in which the correlation between centrality and $\langle N_{part} \rangle$ is estimated in the standard Glauber MC approach [65]. For consistency reasons, for Au-Au collisions ($\sqrt{s_{NN}} = 200$ GeV) we have used both the data published by STAR and PHENIX Collaborations. As one can observe in Figure 4a, there is very good agreement between these two datasets. In order to avoid overloaded figures as much as possible, from now on only the dataset measured by the STAR Collaboration will be used.

The $\langle N_{part} \rangle$ dependence of the suppression has the advantage that at a given $\langle N_{part} \rangle$, the fireball transverse area S_{\perp} is the same for the colliding systems and collision energies in question [66], with small deviations observed at very central collisions in Cu-Cu and Xe-Xe relative to Au-Au and Pb-Pb [38], where the fireball shapes are closer to a circular geometry, qualitatively represented in Figure 5. At LHC energies, with a slight change in the offset (≈ 10 fm²) the linear dependence of S_{\perp} on $\langle N_{part} \rangle$ has the same slope as at the RHIC energy (Figure 3). As it is known, all theoretical models predict a greater suppression with increasing path length and energy density or temperature of the deconfined medium traversed by a parton [15–24]. In Figure 6, the suppression in terms of $(1-R_{AA})$ in the $5 < p_T < 8$ GeV/c region for the colliding systems and energies under consideration, compared with the particle density per unit of rapidity and unit of overlapping area ($\langle dN/dy \rangle / S_{\perp}$), which is a measure of the entropy density and thus of the temperature [26], as a function of $\langle N_{part} \rangle$, is represented. The dN/dy values were estimated as in [38, 39].

In the case of Cu-Cu and Au-Au at $\sqrt{s_{NN}}=200$

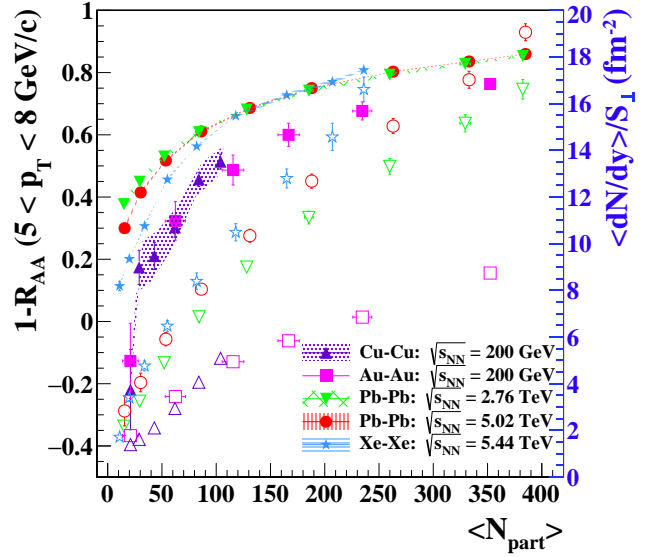


FIG. 6. $(1-R_{AA})$ (full symbols - left scale) and $\langle dN/dy \rangle / S_{\perp}$ (open symbols - right scale) as a function of $\langle N_{part} \rangle$. The abscissa is the same as in Figure 5 and consequently, at a given $\langle N_{part} \rangle$, the full and open symbols correspond to the same fireball shape.

GeV, for the same average number of participants and $\langle dN/dy \rangle / S_{\perp}$, the suppression has the same value, increasing with $\langle dN/dy \rangle / S_{\perp}$ and with the size of the overlapping area. Since the suppression in central Cu-Cu collisions is the same as in Au-Au collisions at the corresponding $\langle N_{part} \rangle$, it appears that the fireball shape plays a minor role, for the same size of the overlapping area, on the azimuthally averaged R_{AA} values. For $\langle N_{part} \rangle=200$, the differences in $\langle dN/dy \rangle / S_{\perp}$ for Pb-Pb at $\sqrt{s_{NN}}=2.76$, 5.02 TeV and for Xe-Xe at $\sqrt{s_{NN}}=5.44$ TeV, relative to Au-Au at $\sqrt{s_{NN}}=200$ GeV, are 5.25 ± 1 , 6.77 ± 1 and 7.89 ± 1 (particles/fm²) while the differences in $(1-R_{AA})$ are 0.10 ± 0.03 , 0.11 ± 0.03 and 0.11 ± 0.03 . This suggests a suppression saturation at LHC energies. For central Au-Au collisions, i.e. $\langle N_{part} \rangle=350$, the difference in $\langle dN/dy \rangle / S_{\perp}$ between Pb-Pb at $\sqrt{s_{NN}}=2.76$ TeV and Au-Au at $\sqrt{s_{NN}}=200$ GeV is 7 ± 1 (particles/fm²) while the difference in $(1-R_{AA})$ is 0.08 ± 0.03 .

Using the phenomenological "abc" parton energy loss approach [67], where the fractional energy loss is:

$$\frac{\Delta E}{E} \propto T^a L^b \quad (6)$$

and the approximation from [68], one obtains:

$$(1 - R_{AA}) \propto \xi T^a L^b, \quad (7)$$

where L is the average path length and T is the average temperature. With the assumption that $L^2 \propto S_{\perp}$, the entropy density $s \propto \langle dN/dy \rangle / S_{\perp}$ and $T^3 \propto \langle dN/dy \rangle / S_{\perp}$ [26], one could estimate ξ for three values of the parameters a and b, used by different models in order to reproduce the experimental results related to the suppression: i) a=1, b=2; ii) a=1, b=1 [68, 69]; iii) a=3, b=2

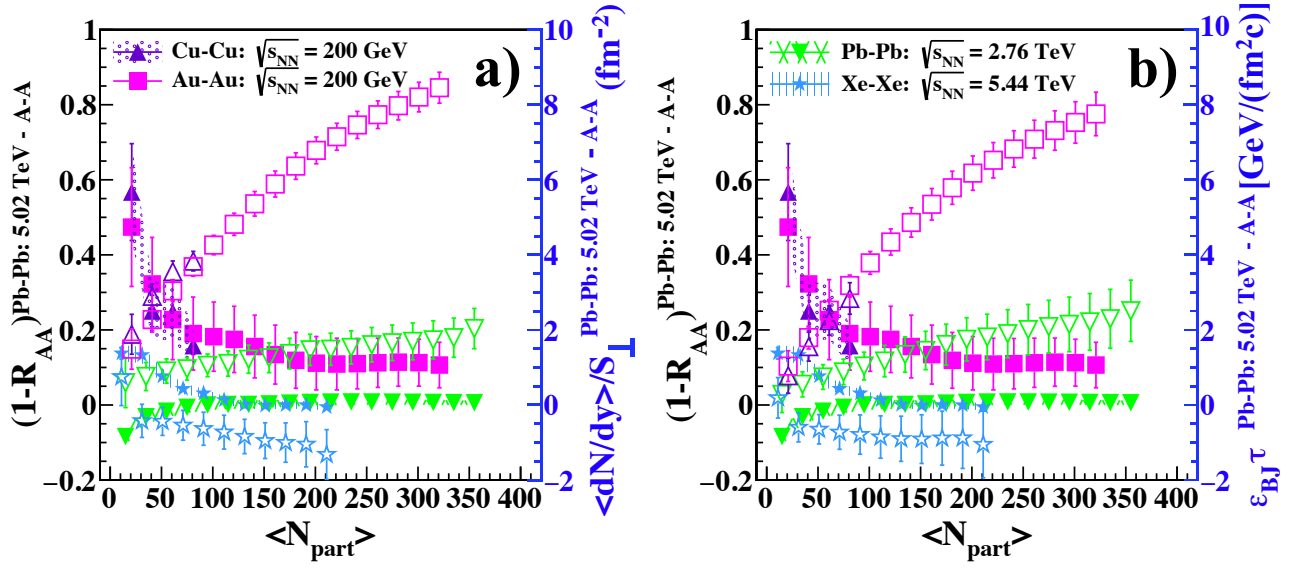


FIG. 7. The difference between the suppression in Pb-Pb at $\sqrt{s_{NN}}=5.02$ TeV and the suppression in Pb-Pb at $\sqrt{s_{NN}}=2.76$ TeV, Xe-Xe at $\sqrt{s_{NN}}=5.44$ TeV, Au-Au and Cu-Cu at $\sqrt{s_{NN}}=200$ GeV (full symbols). The corresponding differences in terms of particle density per unit of rapidity and unit of overlapping area $\langle dN/dy \rangle / S_{\perp}$ (Figure 7a - open symbols) and of Bjorken energy density times the interaction time $\epsilon_{Bj} \cdot \tau$ (Figure 7b - open symbols) at the corresponding collision energies can be followed using the scales on the right sides.

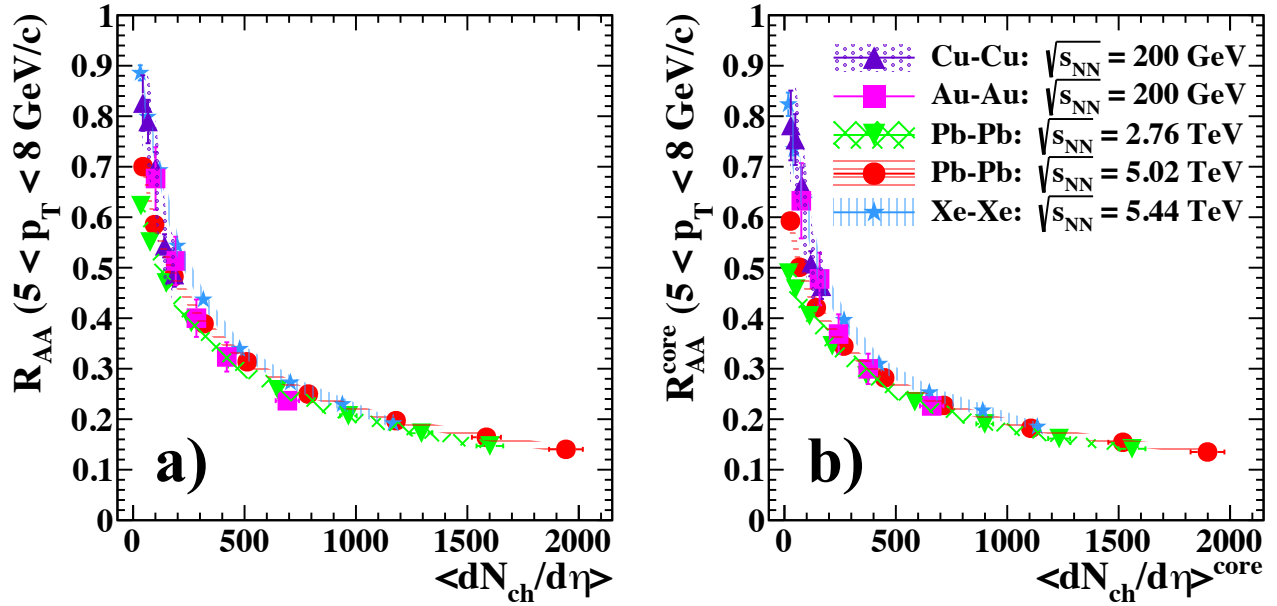


FIG. 8. R_{AA} as a function of charged particle density per unit of pseudorapidity, $\langle dN_{ch}/d\eta \rangle$, for the same systems and collision energies as in Figure 4; a) experimental values; b) the core contribution to R_{AA} and $\langle dN_{ch}/d\eta \rangle_{core}$.

[67]. Using the experimental values of $(1-R_{AA})$ for Au-Au at $\sqrt{s_{NN}}=200$ GeV and Pb-Pb at $\sqrt{s_{NN}}=2.76$ TeV at $\langle N_{part} \rangle=350$, corresponding to the most central collisions for Au-Au at $\sqrt{s_{NN}}=200$ GeV, one obtains: i) $\xi^{LHC} = 0.86(\pm 0.03) \cdot \xi^{RHIC}$; ii) $\xi^{LHC} = 0.88(\pm 0.03) \cdot \xi^{RHIC}$ and iii) $\xi^{LHC} = 0.58(\pm 0.04) \cdot \xi^{RHIC}$. Although theoretically not compelling, as it was mentioned in Ref. [23], we

used ansatz iii) based on their results on relative success and failure of different models (Table 2 and 3 in the same paper). Previous studies [70–72] have shown that the running coupling alters the jet-energy dependence of energy loss and $\frac{\Delta E}{E}$ is approximately independent on E. Obviously, the hydrodynamic expansion of the deconfined matter traversed by the parton plays

a role in the estimated final suppression. Using the $\sqrt{\langle dN/dy \rangle / S_{\perp}}$ scaling of the average transverse flow velocity, $\langle \beta_T \rangle$, reported in Ref. [38], for the geometrical scaling variable corresponding to the particle densities used before for the ξ^{LHC} / ξ^{RHIC} estimation, a ratio $\langle \beta_T \rangle^{LHC} / \langle \beta_T \rangle^{RHIC} \simeq 1.09 \pm 0.08$ is obtained. This could be one of the reasons leading to lower values of the jet-medium coupling in Pb-Pb central collision at $\sqrt{s_{NN}}=2.76$ TeV energy relative to Au-Au central collision at $\sqrt{s_{NN}}=200$ GeV. In Table II ($\langle dN/dy \rangle / S_{\perp}$)^{1/3} $\sim T$, $\langle \beta_T \rangle$ and $(1 - R_{AA})^{\pi^0}$ for the 0-5% collision centrality for Au-Au at $\sqrt{s_{NN}}=39$ GeV and 200 GeV and for Pb-Pb at $\sqrt{s_{NN}}=2.76$ TeV are listed. A comparison between 39 GeV and 200 GeV for Au-Au collisions shows an increase of 39.7% relative to $\sqrt{s_{NN}}=39$ GeV in the suppression, while the increase in ($\langle dN/dy \rangle / S_{\perp}$)^{1/3} and $\langle \beta_T \rangle$ is 20.3% and 20.4%, respectively. The increase in the suppression from $\sqrt{s_{NN}}=200$ GeV (Au-Au) to $\sqrt{s_{NN}}=2.76$ TeV is 7.4% relative to $\sqrt{s_{NN}}=200$ GeV, while the increase in ($\langle dN/dy \rangle / S_{\perp}$)^{1/3} and $\langle \beta_T \rangle$ is 24.2% and 10.2%, respectively. In this case, a ≈ 4 times smaller difference in the suppression, for a larger difference in ($\langle dN/dy \rangle / S_{\perp}$)^{1/3} and a smaller difference in the expansion velocity, can be observed.

TABLE II: ($\frac{\langle dN/dy \rangle}{S_{\perp}}$)^{1/3}, $\langle \beta_T \rangle$ [38] and $(1 - R_{AA})^{\pi^0}$ for the 0-5% collision centrality for Au-Au at $\sqrt{s_{NN}}=39$ GeV and 200 GeV [47, 73] and for Pb-Pb at $\sqrt{s_{NN}}=2.76$ TeV [74].

System	$\sqrt{s_{NN}}$ (GeV)	Cent. (%)	($\frac{\langle dN/dy \rangle}{S_{\perp}}$) ^{1/3}	$\langle \beta_T \rangle$	$(1 - R_{AA})^{\pi^0}$
Au-Au	39	0-5	1.72 \pm 0.03	0.49 \pm 0.04	0.58 \pm 0.02
Au-Au	200	0-5	2.07 \pm 0.03	0.59 \pm 0.05	0.81 \pm 0.06
Pb-Pb	2760	0-5	2.57 \pm 0.04	0.65 \pm 0.06	0.87 \pm 0.08

This supports the assumption that the main contribution to the observed evolution of $(1 - R_{AA})$ as a function of collision energy, i.e. a strong increase followed by a weakening dependence, is due to the energy density (temperature) dependence of the parton energy loss in the deconfined medium. In Figure 7, the relative differences between the suppression in Pb-Pb at $\sqrt{s_{NN}}=5.02$ TeV and the suppression in Au-Au and Cu-Cu collisions at $\sqrt{s_{NN}}=200$ GeV, Pb-Pb collisions at $\sqrt{s_{NN}}=2.76$ TeV and Xe-Xe collisions at $\sqrt{s_{NN}}=5.44$ TeV are shown. The corresponding differences in particle density per unit of rapidity and unit of overlapping area, $\langle dN/dy \rangle / S_{\perp}$ (Figure 7a) and Bjorken energy density times the interaction time, $\epsilon_{Bj} \cdot \tau$ (Figure 7b) are also shown with the corresponding scales on the right side of the figures.

The Bjorken energy density times the interaction time is estimated based on [75]:

$$\epsilon_{Bj} \cdot \tau = \frac{dE_T}{dy} \cdot \frac{1}{S_{\perp}} \quad (8)$$

where E_T is the total transverse energy and S_{\perp} represents the overlapping area of the colliding nuclei. The total transverse energy per unit of rapidity can be estimated as follows:

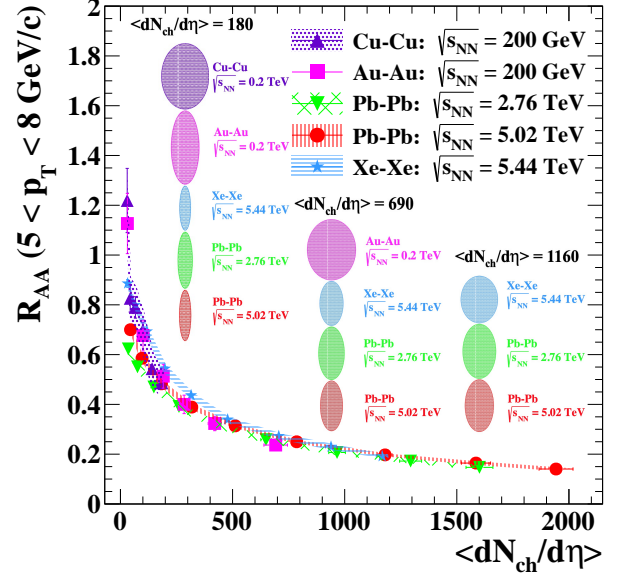


FIG. 9. The same as Figure 8a, with the shapes of the overlapping area S_{\perp} at different values of $\langle dN_{ch}/d\eta \rangle$.

- RHIC $\sqrt{s_{NN}}=200$ GeV:

$$\frac{dE_T}{dy} \approx \frac{3}{2} \left(\langle m_T \rangle \langle \frac{dN}{dy} \rangle \right)_{\pi^{\pm}} + 2 \left(\langle m_T \rangle \langle \frac{dN}{dy} \rangle \right)_{K^{\pm}, p, \bar{p}} \quad (9)$$

- LHC energies:

$$\frac{dE_T}{dy} \approx \frac{3}{2} \left(\langle m_T \rangle \langle \frac{dN}{dy} \rangle \right)_{\pi^{\pm}} + 2 \left(\langle m_T \rangle \langle \frac{dN}{dy} \rangle \right)_{K^{\pm}, p, \bar{p}, \Xi^{\pm}, \Xi^{\pm}} + \left(\langle m_T \rangle \langle \frac{dN}{dy} \rangle \right)_{\Lambda, \bar{\Lambda}, \Omega^{\pm}, \bar{\Omega}^{\pm}} \quad (10)$$

The input data used in the estimation of the Bjorken energy density times the interaction time are reported in [32, 33, 38, 77–82] and Table I.

Within the error bars, the suppression in Pb-Pb collisions at $\sqrt{s_{NN}}=2.76$ TeV is the same with the one corresponding to $\sqrt{s_{NN}}=5.02$ TeV for all values of $\langle N_{part} \rangle$, although the difference in $\langle dN/dy \rangle / S_{\perp}$ and in $\epsilon_{Bj} \cdot \tau$ increases from 0.88 ± 0.33 particles/ fm^2 to 1.95 ± 0.54 particles/ fm^2 and from 0.71 ± 0.32 GeV/(fm^2c) to 2.44 ± 0.81 GeV/(fm^2c), respectively, from the low ($\langle N_{part} \rangle=50$) to the highest value of $\langle N_{part} \rangle$ ($\langle N_{part} \rangle=350$). The difference between the suppression in Pb-Pb at $\sqrt{s_{NN}}=5.02$ TeV and Au-Au at $\sqrt{s_{NN}}=200$ GeV decreases from 0.27 ± 0.25 to 0.08 ± 0.02 with $\langle N_{part} \rangle$, while the differences in $\langle dN/dy \rangle / S_{\perp}$ and $\epsilon_{Bj} \cdot \tau$ increase from 2.63 ± 0.29 particles/ fm^2 and 2.13 ± 0.28 GeV/(fm^2c) to 8.9 ± 0.43 particles/ fm^2 and 8.2 ± 0.8 GeV/(fm^2c), respectively.

An alternative representation of R_{AA} could be done as a function of the average charged particle density per unit of pseudorapidity [35]. The $\langle dN_{ch}/d\eta \rangle$ experimental data

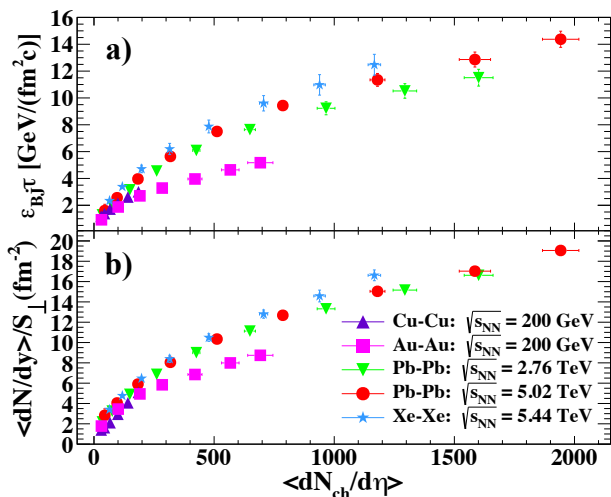


FIG. 10. a) The Bjorken energy density times the interaction time $\epsilon_{Bj} \cdot \tau$; b) particle density per unit of rapidity and unit of overlapping area $\langle dN/dy \rangle / S_{\perp}$, both as a function of the average charged particle density per unit of pseudorapidity $\langle dN_{ch}/d\eta \rangle$.

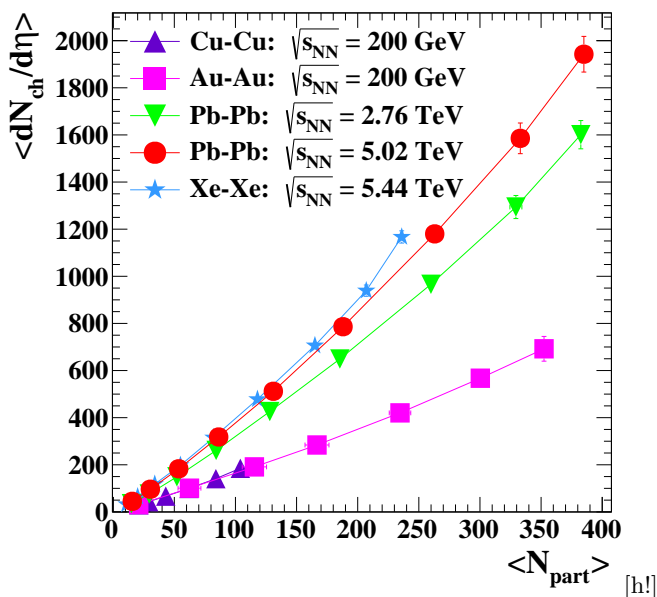


FIG. 11. The average charged particle density per unit of pseudorapidity $\langle dN_{ch}/d\eta \rangle$ as a function of the average value of participating nucleons $\langle N_{part} \rangle$.

for heavy ion collisions are taken from [32, 33, 35, 36, 83]. The R_{AA} as a function of $\langle dN_{ch}/d\eta \rangle$ is presented in Figure 8a for the same systems and collision energies as in Figure 4. In such a representation, all systems at all energies scale as a function of $\langle dN_{ch}/d\eta \rangle$. The same representation in terms of R_{AA}^{core} and $\langle dN_{ch}/d\eta \rangle^{core}$ (Figure 8b) shows a larger deviation between RHIC and LHC energies for $\langle dN_{ch}/d\eta \rangle \leq 200$. Relative to the $\langle N_{part} \rangle$ dependence, the difference in the shapes of the overlapping areas of different systems for a given $\langle dN_{ch}/d\eta \rangle$ is

larger, as it can be seen in Figure 9. If we look at the dependence of $\epsilon_{Bj} \cdot \tau$ or $\langle dN/dy \rangle / S_{\perp}$ respectively as a function of charged particle density (Figure 10a and Figure 10b), a difference between the collision energies which increases with $\langle dN_{ch}/d\eta \rangle$ is seen.

Therefore, with several contributions playing a role in the observed scaling in $\langle dN_{ch}/d\eta \rangle$, it is rather difficult to unravel the importance of each one of them. The difference between the two representations is explained by the correlation between $\langle dN_{ch}/d\eta \rangle$ and $\langle N_{part} \rangle$, presented in Figure 11. While the overlapping area depends little on the system size and collision energy for a given $\langle N_{part} \rangle$ [38], $\langle dN_{ch}/d\eta \rangle$ combines the contribution of both collision energy and system size.

IV. WHY R_{AA}^N ?

R_{AA} , as a measure of the suppression in heavy ion collisions, is based on the estimate of the number of binary collisions $\langle N_{bin} \rangle$ within the Glauber MC approach using straight trajectories as a hypothesis. The dependence on the collision energy is introduced by the nucleon-nucleon cross section and the oversimplified assumption that every nucleon-nucleon collision takes place at the same energy, \sqrt{s} , and consequently the same cross section, σ_{pp} . In Figure 12, the correlation between the number of binary collisions $\langle N_{bin} \rangle$ and $\langle N_{part} \rangle$ estimated within the standard Glauber MC approach is represented.

An alternative approach, where the energy and σ_{pp} change after each collision [84], has shown that in Pb-Pb collisions at $\sqrt{s_{NN}}=2.76$ TeV, the average number of binary collisions $\langle N_{bin} \rangle$ is significantly lower than the values estimated by the standard Glauber model with the difference increasing towards central collisions. The difference in $\langle N_{part} \rangle$ is negligible at peripheral and central collisions. For mid-central collisions it is about 18%.

$\langle N_{bin} \rangle / [\langle dN_{ch}/d\eta \rangle^{A-A} / \langle dN_{ch}/d\eta \rangle^{pp,MB}]$ has to be unity if only single collisions take place. A very good correlation between $\langle N_{bin} \rangle$ estimated within the standard Glauber model and experimental values of $\langle dN_{ch}/d\eta \rangle^{A-A} / \langle dN_{ch}/d\eta \rangle^{pp,MB}$ is evidenced in Figure 13. However, their ratio as a function of $\langle N_{part} \rangle$ shows an increase from close to 1 for the lowest values of $\langle N_{part} \rangle$, up to $\langle N_{part} \rangle \approx 150$, followed by a tendency towards a saturation at ≈ 3.5 for the largest $\langle N_{part} \rangle$ values (Figure 14). All systems at all investigated energies overlap in this representation. In the case of pp collisions, $\langle dN_{ch}/d\eta \rangle^{INEL}$ corresponding to the selection of inelastic collisions and the parametrisation given in [85] had been used.

Based on these, we will also analyse the model independent quantity, namely R_{AA}^N , obtained as a ratio of the p_T spectra in A-A collisions to the one in MB pp collisions at the same energy, with each of them normalised to the corresponding charged particle densities, for all the available centralities in A-A collisions (Eq.(11)). This observable was used in a previous paper for comparing the behaviour of p_T spectra in pp, p-Pb and Pb-Pb col-

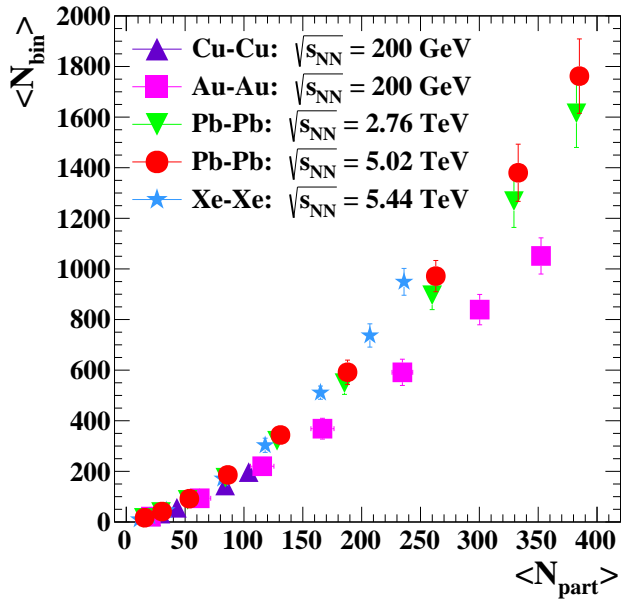


FIG. 12. Correlation between the average number of binary collisions $\langle N_{bin} \rangle$ and the average number of participating nucleons $\langle N_{part} \rangle$ estimated using the Glauber MC approach.

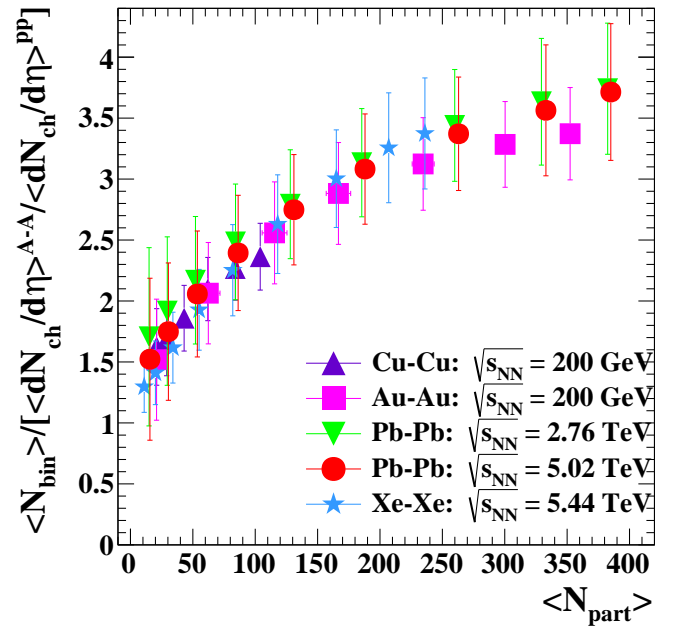


FIG. 14. $\langle N_{bin} \rangle / [(\langle dN_{ch}/d\eta \rangle)^{A-A} / (\langle dN_{ch}/d\eta \rangle)^{pp}]$ as a function of $\langle N_{part} \rangle$.

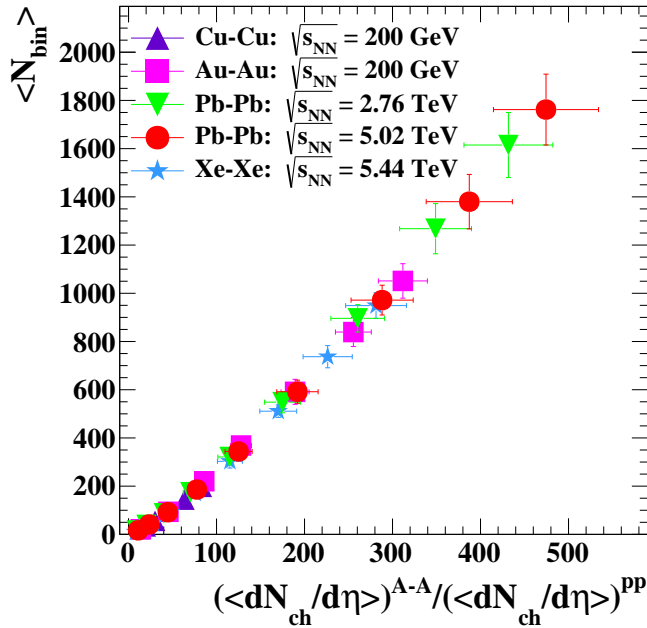


FIG. 13. Correlation between the average number of binary collisions $\langle N_{bin} \rangle$ and experimental $(\langle dN_{ch}/d\eta \rangle)^{AA} / (\langle dN_{ch}/d\eta \rangle)^{pp}$.

lisions as a function of charged particle multiplicity and centrality, respectively [27].

$$R_{AA}^N = \frac{(\frac{d^2 N}{dp_T d\eta} / \langle \frac{dN_{ch}}{d\eta} \rangle)^{cen}}{(\frac{d^2 N}{dp_T d\eta} / \langle \frac{dN_{ch}}{d\eta} \rangle)^{pp,MB}} \quad (11)$$

In Figure 15, R_{AA}^N as a function of $\langle N_{part} \rangle$ for the sys-

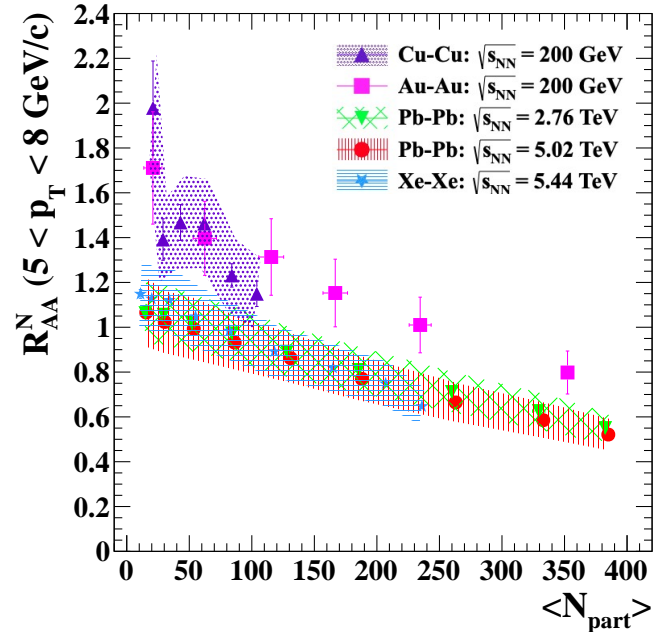


FIG. 15. R_{AA}^N as a function of $\langle N_{part} \rangle$.

tems discussed in the previous section is presented. The system size scaling for each energy domain, i.e. the highest energy at RHIC and LHC energies remains. R_{AA}^N has a close to linear dependence as a function of $\langle N_{part} \rangle$ and at larger values of the average number of participating nucleons, the suppression is reduced compared to R_{AA} . As it is observed in Figure 16, the scaling of R_{AA}^N has not the same quality as R_{AA} as a function of

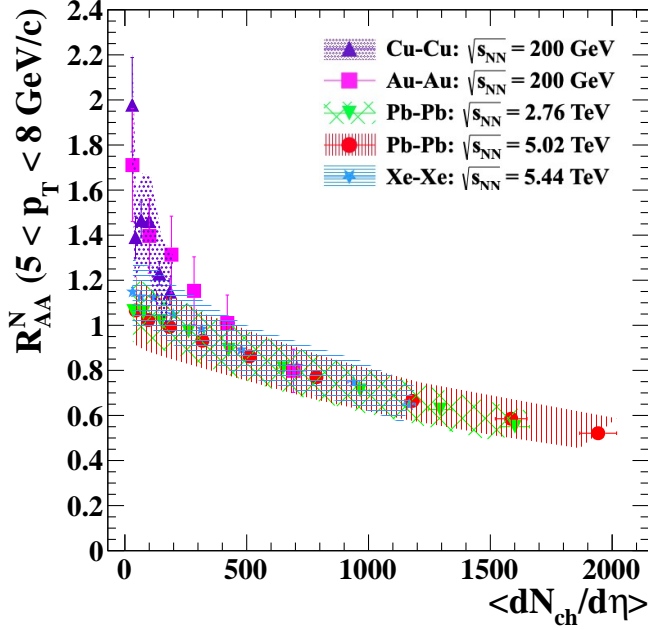


FIG. 16. R_{AA}^N as a function of $\langle dN_{ch}/d\eta \rangle$.

$\langle dN_{ch}/d\eta \rangle$ (see Figure 8a) for the two collision energy domains. However, the scaling at LHC energies remains, a close to linear dependence being evidenced in this representation as well. The same considerations as in Section III can be used in order to estimate the expected suppression, $(1-R_{pp}^{N(HM)})$, for pp collisions at $\sqrt{s}=7$ TeV and very high charged particle multiplicity (HM) events. The geometrical scaling [38] shows that for the highest charged particle multiplicity in pp collisions at $\sqrt{s}=7$ TeV, in the case of $\alpha=1$, $\sqrt{\langle dN/dy \rangle/S_{\perp}}=3.3 \pm 0.1$ particles $\cdot fm^{-1}$, $\langle \beta_T \rangle$ in pp and Pb-Pb at $\sqrt{s_{NN}}=2.76$ TeV is the same. Therefore, the contribution of the hydrodynamic expansion to the suppression should play a similar role. For this value of $\sqrt{\langle dN/dy \rangle/S_{\perp}}$, $S_{\perp}^{pp}(\alpha=1)=7.43 \pm 0.48 fm^2$ and $S_{\perp}^{Pb-Pb}=70 \pm 0.4 fm^2$ (corresponding to $\langle N_{part} \rangle=125$). Assuming the same jet-medium coupling, $(1-R_{pp}^{N(HM)})/(1-R_{AA}^N(\langle N_{part} \rangle=125)) \approx S_{\perp}^{pp,HM}/S_{\perp}^{Pb-Pb,\langle N_{part} \rangle=125}=0.11 \pm 0.01$. This could explain why in pp collisions at LHC, in high charged particle multiplicity events, in the limit of current experimental uncertainties, no suppression was observed, although similarities to Pb-Pb collisions for other observables were evidenced.

V. RELATIVE SUPPRESSION IN TERMS OF R_{CP}

For energies where the p_T spectra in pp collisions were not measured, the suppression was studied in terms of R_{CP} , i.e. the ratio of charged particle p_T spectra at a given centrality to the p_T spectrum in peripheral colli-

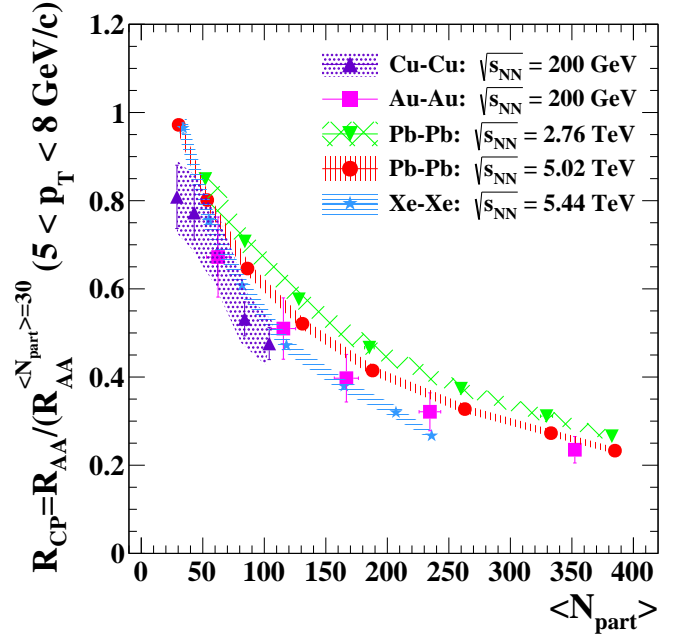


FIG. 17. R_{CP} for Au-Au and Cu-Cu at $\sqrt{s_{NN}}=200$ GeV, Pb-Pb at $\sqrt{s_{NN}}=2.76$ TeV and 5.02 TeV and Xe-Xe at $\sqrt{s_{NN}}=5.44$ TeV, as a function of $\langle N_{part} \rangle$.

sions, each of them divided by the corresponding average number of the binary collisions:

$$R_{CP} = \left(\frac{d^2 N}{d\eta dp_T} \right)^{cen} / \left(\frac{d^2 N}{d\eta dp_T} \right)^{peripheral} \quad (12)$$

for each centrality in A-A collisions.

For a better comparison of the R_{CP} values as a function of $\langle N_{part} \rangle$, the peripheral collision of reference was chosen to be the same for all systems and all energies, i.e. $\langle N_{part} \rangle=30$. The R_{CP} estimated in this way is represented in Figure 17 for the same systems and energies. As in the case of R_{AA} , due to the same reasons, using experimental data, we estimated the R_{CP}^N :

$$R_{CP}^N = \left(\frac{d^2 N}{d\eta dp_T} \right)^{cen} / \left(\frac{d^2 N}{d\eta dp_T} \right)^{peripheral} \quad (13)$$

The R_{CP}^N suppression as a function of $\langle N_{part} \rangle$ (Figure 18) is the same at all values of $\langle N_{part} \rangle$ for all the heavy systems, Au-Au, Xe-Xe and Pb-Pb, although the difference in the collision energies is ≈ 14 -27 times higher at LHC than at RHIC and between the LHC energies is a factor of ≈ 2 . The linear dependence as a function of $\langle N_{part} \rangle$ follows the linear dependence observed in R_{AA}^N .

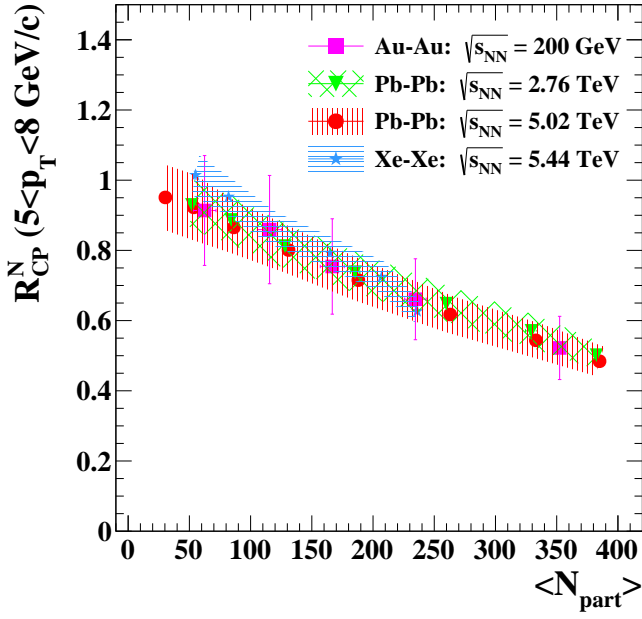


FIG. 18. R_{CP}^N for Au-Au at $\sqrt{s_{NN}}=200$ GeV, Xe-Xe at $\sqrt{s_{NN}}=5.44$ TeV and Pb-Pb at $\sqrt{s_{NN}}=2.76$ TeV and 5.02 TeV as a function of $\langle N_{part} \rangle$.

VI. $(1-R_{AA})/\langle dN/dy \rangle$ AND $(1-R_{AA}^N)/\langle dN/dy \rangle$ DEPENDENCE ON $(\langle dN/dy \rangle/S_{\perp})^{1/3}$

Based on Eq. (7) and ansatz (iii) from Section III and taking $S_{\perp} \propto L^2$, ξ , which is a rough estimate of the jet-coupling constant, turns out to be proportional to $(1-R_{AA})/\langle dN/dy \rangle$. A qualitative temperature dependence of ξ can be obtained from experimental data, as $T \sim (\langle dN/dy \rangle/S_{\perp})^{1/3}$.

As can be seen in Figure 19, $(1-R_{AA})/\langle dN/dy \rangle$ shows an exponential decrease as a function of $(\langle dN/dy \rangle/S_{\perp})^{1/3}$. The hatched line is the result of the fit with the following expression:

$$\frac{1-R_{AA}}{\langle dN/dy \rangle} = e^{\alpha - \beta \cdot (\langle dN/dy \rangle/S_{\perp})^{1/3}} \quad (14)$$

Such a temperature dependence of the jet-medium coupling was considered in Ref.[23] in order to reproduce the nuclear modification factors at RHIC and LHC energies. A similar representation for R_{AA}^N instead of R_{AA} is presented in Figure 20. In this case, $(1-R_{AA}^N)/\langle dN/dy \rangle$ is constant as a function of $(\langle dN/dy \rangle/S_{\perp})^{1/3}$, for $(\langle dN/dy \rangle/S_{\perp})^{1/3} \geq 2.1$ particles/fm^{2/3}, independent on the size of the colliding systems and collision energy. An impact parameter independence of the jet quenching parameter was claimed in a series of theoretical estimates [86–88].

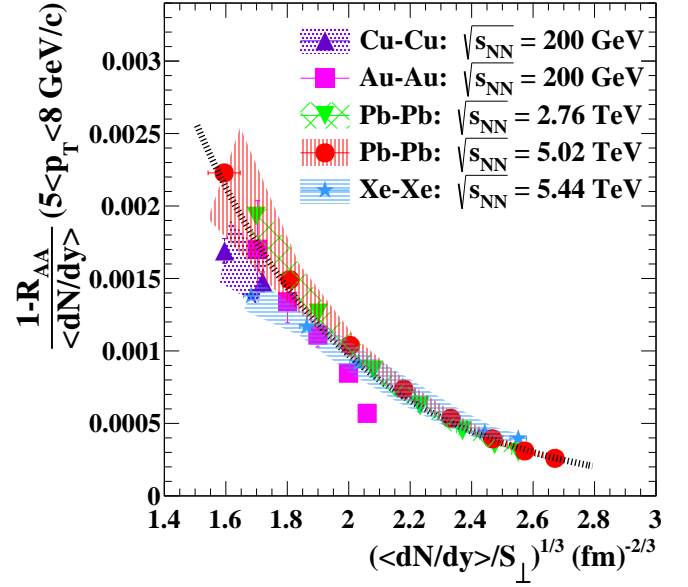


FIG. 19. $(1-R_{AA})/\langle dN/dy \rangle$ dependence on $(\langle dN/dy \rangle/S_{\perp})^{1/3}$. The line is the result of the fit with the expression (14).

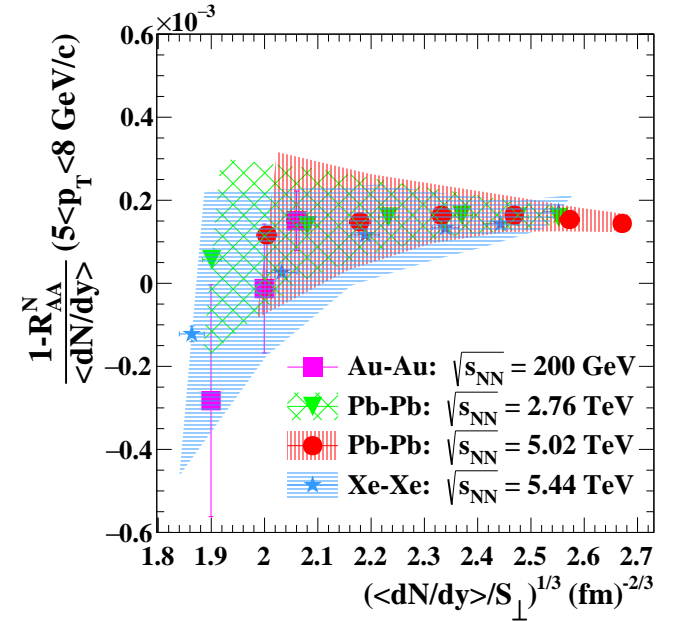


FIG. 20. $(1-R_{AA}^N)/\langle dN/dy \rangle$ dependence on $(\langle dN/dy \rangle/S_{\perp})^{1/3}$.

VII. THE $\sqrt{s_{NN}}$ DEPENDENCE OF R_{CP} , R_{CP}^N , R_{AA}^0 , $(R_{AA}^N)^{\pi^0}$

As it is well known, within the Beam Energy Scan (BES) program at RHIC, valuable data were obtained relative to the behaviour of different observables in Au-Au collisions, starting from $\sqrt{s_{NN}}=7.7$ GeV, up to 39 GeV. Since the p_T spectra for charged particles in pp collisions at these energies were not measured, the STAR Collaboration studied the p_T dependence of R_{CP} [(0-

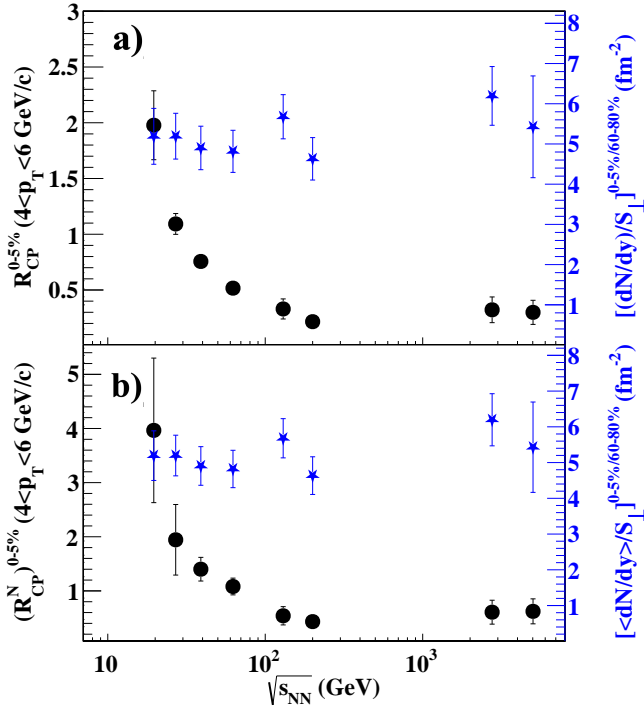


FIG. 21. a) R_{CP} and b) R_{CP}^N , for $4 < p_T < 6$ GeV/c, as a function of $\sqrt{s_{NN}}$ for 0-5% centrality relative to 60-80%, for charged particles in Au-Au and Pb-Pb collisions. On the right scales, the ratio of particle densities per unit of rapidity and unit of overlapping area for the same centralities is given.

5%)/(60-80%]] for different collision energies, for Au-Au collisions [89]. In order to include as much as possible the lower energies, where the published data are in a lower p_T range, we had to change the p_T range from $5 < p_T < 8$ GeV/c, used in previous sections, to $4 < p_T < 6$ GeV/c, for the study of the charged particle suppression dependence on the collision energy. These results, together with the values obtained in Pb-Pb collisions at $\sqrt{s_{NN}}=2.76$ and 5.02 TeV, for the most central collisions, are presented in Figure 21a. Following the arguments from the previous section, R_{CP}^N as a function of the collision energy is presented in Figure 21b. In both plots is evidenced a decrease of R_{CP} or R_{CP}^N from $\sqrt{s_{NN}}=19.6$ GeV up to $\sqrt{s_{NN}}=200$ GeV, while the relative ratios of particle densities per unit of rapidity and unit of overlapping area are constant, within the error bars. Beyond the RHIC energies, R_{CP} and R_{CP}^N remain constant. Since R_{AA} for charged particles at lower RHIC energies are not reported, in order to confirm the above observations, we used the R_{AA} of π^0 published by the PHENIX collaboration at $\sqrt{s_{NN}}=39, 62.4$ and 200 GeV [47, 73] and by the ALICE Collaboration [74, 90] at LHC energies.

In order to have an estimate on $R_{AA}^{\pi^0}$ corresponding to 0-10% centrality for the collision energies where it was not published, we applied the procedure described below. The $\sqrt{s_{NN}}$ dependence of R_{CP} (Figure 21a) was fit

with the following empirical expression:

$$R_{CP} \propto a + \frac{b}{s_{NN}} + c \cdot \sqrt{s_{NN}} \quad (15)$$

with a, b, and c as free parameters, the result being presented in Figure 22a. A similar expression was used in order to fit the measured experimental data of the $R_{AA}^{\pi^0}$ - $\sqrt{s_{NN}}$ dependence (Figure 22b - full symbols), leaving the parameters free. The result was used for estimating $R_{AA}^{\pi^0}$ at the missing collision energies, i.e. 19.6, 27 and 130 GeV (Figure 22b - open symbols). Measured, interpolated and extrapolated $R_{AA}^{\pi^0}$ values as a function of $\sqrt{s_{NN}}$ are presented in Figure 23, for both p_T ranges used in this paper, namely 4-6 GeV/c (open symbols) and 5-8 GeV/c (full symbols).

The $R_{AA}^{\pi^0}$ dependence as a function of $\sqrt{s_{NN}}$ is qualitatively similar with the one evidenced for R_{CP} corresponding to charged particles presented in Figure 21a. The suppression starts around $\sqrt{s_{NN}}=27$ GeV, becomes more significant up to the top RHIC energy and remains constant up to the LHC energies. The ratios relative to $\langle dN/dy \rangle$ as a function of collision energy are presented in Figure 24, namely: $(1 - R_{AA}^{\pi^0})/\langle dN/dy \rangle$ (Figure 24a) and $[1 - (R_{AA}^N)^{\pi^0}]/\langle dN/dy \rangle$ (Figure 24b).

These ratios show a maximum around the top RHIC energies (in the region of $\sqrt{s_{NN}} = 62.4 - 130$ GeV), decreasing towards LHC energies, in qualitative agreement with theoretical predictions [22, 25, 91]. To what extent such a trend is due to a transition from a magnetic plasma of light monopoles near the critical temperature region [91] to a deconfined matter dominated by quarks and gluons [25] remains an open question. However, the trends in the experimental data suggest a change in the properties of the deconfined matter from RHIC to LHC energies.

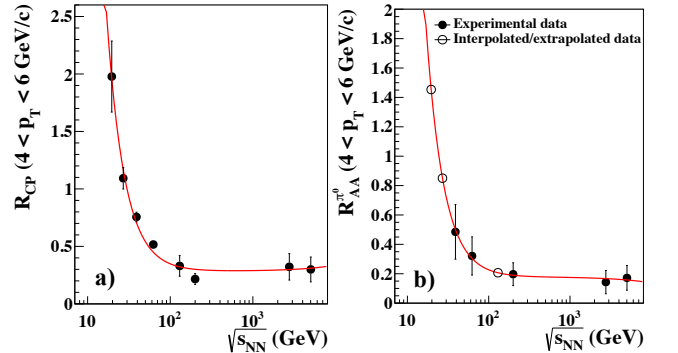


FIG. 22. a) The same as Figure 21a. b) R_{AA} for π^0 , corresponding to the same range in p_T as a), for experimental values (full symbols) and interpolated/extrapolated results (open symbols) for 0-10% centrality. In both plots the continuous line is the fit with Eq.15.

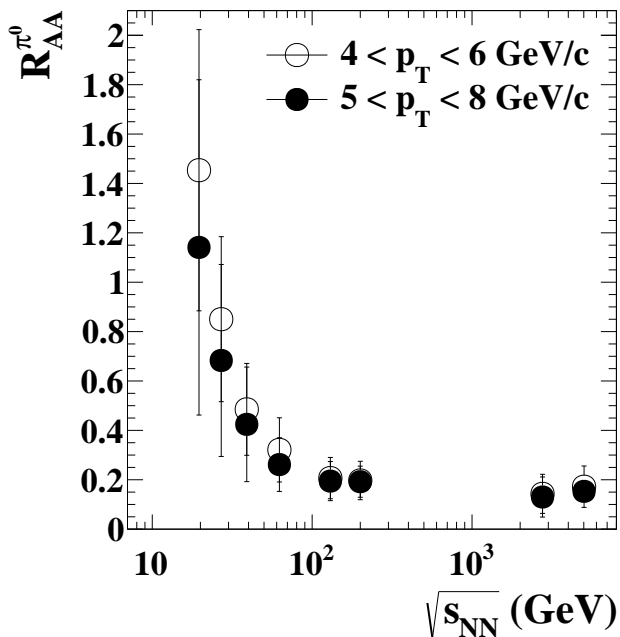


FIG. 23. π^0 R_{AA} for the two p_T ranges: 4-6 GeV/c (open symbols) and 5-8 GeV/c (full symbols) for 0-10% centrality.

VIII. CONCLUSIONS

The present paper is mainly based on published experimental data obtained at RHIC and LHC. The motivation of this was to study possible scaling or distinctive features between the two energy regimes. Without claiming precise calculations that are extremely laborious, we tried to rely mainly on experimental considerations. Based on the experimental results obtained at RHIC for Au-Au, Cu-Cu and at LHC for Pb-Pb and Xe-Xe collisions, a detailed analysis of the charged particle suppression in the region of transverse momentum corresponding to the maximum suppression is presented.

In order to draw conclusions independent of estimates of the number of binary collisions used in the definitions of R_{AA} and R_{CP} , we define the quantities R_{AA}^N and R_{CP}^N in which the ratios of p_T spectra are normalised to charged particle density ($dN_{ch}/d\eta$) before they are then divided by the relevant pp or peripheral p_T spectra, again normalised by charged particle density in pp or peripheral collision.

While R_{AA} scales as a function of $\langle dN_{ch}/d\eta \rangle$ for the top RHIC and all LHC energies, it scales separately as a function of $\langle N_{part} \rangle$ for RHIC and LHC energies, for all the corresponding measured colliding systems. However, given that $\langle dN_{ch}/d\eta \rangle$ depends on the collision energy and on the overlapping area of the colliding systems, their relative contribution to suppression is rather difficult to unravel. This is the main reason why the considerations on the suppression phenomena as a function of collision geometry and collision energy are mainly based on the $\langle N_{part} \rangle$ dependence.

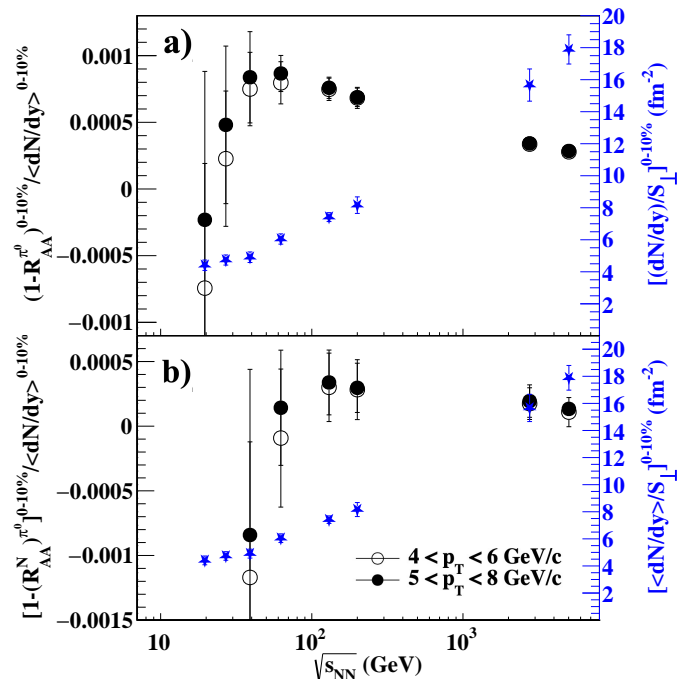


FIG. 24. a) $(1 - R_{AA}^{\pi^0})/\langle dN/dy \rangle$ as a function of collision energy; b) $(1 - (R_{AA}^N)^{\pi^0})/\langle dN/dy \rangle$ as a function of collision energy (bullets)-left scale and $(\langle dN/dy \rangle/S_{\perp})$ (stars)-right scales for the 0-10% centrality.

The influence of the corona contribution on the experimental R_{AA} is presented. As expected, the main corona contribution is at low values of $\langle N_{part} \rangle$ where the core suppression relative to the experimental value is larger.

Based on $(1 - R_{AA})$ and $\langle dN/dy \rangle/S_{\perp} \sim T^3$ dependences on $\langle N_{part} \rangle$, one could conclude that a saturation of suppression at LHC energies takes place. At $\langle N_{part} \rangle = 350$, corresponding to the most central Au-Au collisions at $\sqrt{s_{NN}} = 200$ GeV, if one considers the parton energy loss proportional with the squared path length and with the particle density per unit of rapidity and unit of overlapping area, the proportionality factor ξ is approximately two times lower at LHC than at RHIC. The difference in the hydrodynamic expansion extracted from the $\langle \beta_T \rangle$ scaling as a function of $\sqrt{\langle dN/dy \rangle}/S_{\perp}$ cannot explain this difference. Such considerations, applied to the highest charged particle multiplicity measured in pp collisions at 7 TeV could explain why no suppression is evidenced in such events, in the limit of current experimental uncertainties, while there are similarities to Pb-Pb with respect to other observables. R_{AA}^N as a function of $\langle N_{part} \rangle$ shows similar separate scaling for RHIC and LHC energies, with a linear dependence being evidenced. R_{CP}^N shows a very good scaling as a function of $\langle N_{part} \rangle$ for the heavy systems at all collision energies. The ratio $(1 - R_{AA})/\langle dN/dy \rangle$ shows an exponential decrease with $(\langle dN/dy \rangle/S_{\perp})^{1/3}$ while $(1 - R_{AA}^N)/\langle dN/dy \rangle$ is independent on $(\langle dN/dy \rangle/S_{\perp})^{1/3}$ for $(\langle dN/dy \rangle/S_{\perp})^{1/3} \geq 2.1$ particles/fm^{2/3}, the value being

the same for all the heavy systems at all the collision energies, showing the possible dependence of the jet-medium coupling as a function of temperature. For the most central collisions, R_{CP} , R_{CP}^N for charged particles and $R_{AA}^{\pi^0}$, $(R_{AA}^N)^{\pi^0}$ for $4 < p_T < 6$ GeV/c and $5 < p_T < 8$ GeV/c, measured at RHIC in Au-Au collisions and at LHC in Pb-Pb collisions, evidence, as a function of the collision energy, an increase of the suppression from $\sqrt{s_{NN}} = 39$ GeV up to 200 GeV, followed by a saturation up to the highest energy, $\sqrt{s_{NN}} = 5.02$ TeV for Pb-Pb collisions. $(1 - R_{AA}^{\pi^0})/\langle dN/dy \rangle$ and $[1 - (R_{AA}^N)^{\pi^0}]/\langle dN/dy \rangle$ for the

0-10% centrality evidence a maximum around the largest RHIC energies, in qualitative agreement with models predictions. To what extent this pattern is a signature of a transition in the deconfined matter properties from the top RHIC energy to LHC energies has to be further confirmed by theoretical models.

ACKNOWLEDGMENTS

This work was carried out under the contracts sponsored by the Ministry of Education and Research: RONIPALICE-04/10.03.2020 (via IFA Coordinating Agency) and PN-19 06 01 03.

-
- [1] I.C. Arsene et al. (BRAHMS Collaboration). *Nucl.Phys.A*, 757:1, 2005.
- [2] B.B. Back et al. (PHOBOS Collaboration). *Nucl.Phys.A*, 757:28, 2005.
- [3] J. Adams et al. (STAR Collaboration). *Nucl.Phys.A*, 757:102, 2005.
- [4] K. Adcox et al. (PHENIX Collaboration). *Nucl.Phys.A*, 757:184, 2005.
- [5] J.T. Mitchell et al. (PHENIX Collaboration). *Nucl.Phys.A*, 904-905:903c, 2013.
- [6] D. McDonald et al. (STAR Collaboration). *Eur.Phys.J.Web of Conferences*, 95:01009, 2015.
- [7] J.C. Collins and M.J. Perry. *Phys.Rev.Lett.*, 34:1353, 1975.
- [8] G.F. Chapline and A.K. Kerman. *MIT report CTP-695*, 1978.
- [9] E.V. Shuryak. *Phys.Lett.B*, 78:150, 1978.
- [10] S.A. Chin. *Phys.Lett.B*, 78:552, 1978.
- [11] J.D. Bjorken. *FERMILAB-PUB-82-059-THY*, 1982.
- [12] D. d'Enterria and B. Betz. *Lecture Notes in Physics*, 785:285, 2010.
- [13] D. d'Enterria. *Relativistic Heavy Ion Physics, Landolt-Börnstein - Group I Elementary Particles, Nuclei and Atoms, Springer-Verlag Berlin Heidelberg, ISBN 978-3-642-01538-0*, 23:471, 2010.
- [14] T. Renk. *Phys.Rev.C*, 76:064905, 2007.
- [15] R. Baier et al. *Nucl.Phys.B*, 483:291, 1997.
- [16] M. Gyulassy, P. Levai, and I. Vitev. *Nucl.Phys.B*, 571:197, 2000.
- [17] R. Baier et al. *J. High Energ. Phys.*, 0109:033, 2001.
- [18] F. Arleo. *J. High Energ. Phys.*, 11:044, 2002.
- [19] B. Müller and K. Rajagopal. *Eur.Phys.J.*, C43:15, 2005.
- [20] M. Djordjevic and U.W. Heinz. *Phys.Rev.Lett.*, 101:022302, 2008.
- [21] J. Casalderrey-Solana et al. *J. High Energ. Phys.*, 09:175, 2015.
- [22] K.M. Burke et al. (JET Collaboration). *Phys.Rev.C*, 90:014909, 2014.
- [23] B. Betz and M. Gyulassy. *J. High Energ. Phys.*, 08:090, 2014.
- [24] F. Arleo and G. Falmagne. *PoS(HardProbes2018)*, page 075, 2018.
- [25] S. Shi, J. Liao, and M. Gyulassy. *Chinese Phys. C*, 43:044101, 2019.
- [26] Ramona Vogt. *Ultrarelativistic Heavy-Ion Collisions*, Elsevier Science:ISBN 978-0-444-52196-5, 2007.
- [27] M. Petrovici et al. *AIP Conference Proceedings*, 1852:050003, 2017.
- [28] R.J. Glauber. *Phys. Rev.*, 100:242, 1955.
- [29] V. Franco and R.J. Glauber. *Phys. Rev.*, 142:119, 1966.
- [30] M.L. Miller et al. *Ann.Rev.Nucl.Part.Sci.*, 57:205, 2007.
- [31] M. Rybczynski et al. *Comput. Phys. Commun.*, 185:1759, 2014.
- [32] B.I. Abelev et al. (STAR Collaboration). *Phys.Rev.C*, 79:034909, 2009.
- [33] B. Abelev et al. (ALICE Collaboration). *Phys.Rev.C*, 88:044910, 2013.
- [34] C. Loizides et al. *arXiv:1408.2549v9[nucl-ex]*, 2019.
- [35] S. Acharya et al. (ALICE Collaboration). *Phys.Lett.B*, 788:166, 2019.
- [36] J. Adam et al. (ALICE Collaboration). *Phys.Rev.Lett.*, 116:222302, 2016.
- [37] B. Alver et al. *Phys.Rev.C*, 77:014906, 2008.
- [38] M. Petrovici et al. *Phys.Rev.C*, 98:024904, 2018.
- [39] M. Petrovici et al. *AIP Conference Proceedings*, 2076:040001, 2019.
- [40] B. Alver et al. (PHOBOS Collaboration). *Phys.Rev.Lett.*, 96:212301, 2006.
- [41] J. Adams et al. (STAR Collaboration). *Phys.Rev.Lett.*, 91:172302, 2003.
- [42] S. Acharya et al. (ALICE Collaboration). *Phys.Lett.B*, 790:35, 2019.
- [43] J. Adam et al. (ALICE Collaboration). *Phys.Rev.C*, 94:034903, 2016.
- [44] S.S. Adler et al. (PHENIX Collaboration). *Phys.Rev.C*, 69:034910, 2004.
- [45] B.B. Back et al. *Phys.Rev.Lett.*, 94:082304, 2005.
- [46] B.I. Abelev et al. (STAR Collaboration). *Phys.Rev.C*, 81:054907, 2010.
- [47] A. Adare et al. (PHENIX Collaboration). *Phys.Rev.Lett.*, 109:152301, 2012.
- [48] A.M. Sirunyan et al. (CMS Collaboration). *J. High Energ. Phys.*, 10:138, 2018.
- [49] S. Chatrchyan et al. (CMS Collaboration). *Eur.Phys.J.*, C72:1945, 2012.
- [50] B. Abelev et al. (ALICE Collaboration). *Phys.Lett.B*, 720:52, 2013.
- [51] G. Aad et al. (ATLAS Collaboration). *J. High Energ. Phys.*, 09:050, 2015.

- [52] S. Acharya et al. (ALICE Collaboration). *J. High Energy Phys.*, 1811:013, 2018.
- [53] F. Becattini et al. *Phys.Rev.C*, 69:024905, 2004.
- [54] P. Bozek. *Acta Phys. Pol.*, B36:3071, 2005.
- [55] K. Werner. *Phys.Rev.Lett.*, 98:152301, 2007.
- [56] J. Steinheimer and M. Bleicher. *Phys.Rev.C*, 84:024905, 2011.
- [57] F. Becattini and J. Manninen. *J.Phys.G*, 35:104013, 2008.
- [58] F. Becattini and J. Manninen. *Phys.Lett.B*, 673:19, 2009.
- [59] J. Aichelin and K. Werner. *Phys.Rev.C*, 79:064907, 2009.
- [60] J. Aichelin and K. Werner. *Phys.Rev.C*, 82:034906, 2010.
- [61] P. Bozek. *Phys.Rev.C*, 79:054901, 2009.
- [62] K. Werner C. Schreiber and J. Aichelin. *Phys. Atom. Nucl.*, 75:640, 2012.
- [63] M. Gemard and J. Aichelin. *Astron. Nachr.*, 335:660, 2014.
- [64] M. Petrovici et al. *Phys.Rev.C*, 96:014908, 2017.
- [65] C. Loizides and A. Morsch. *Phys.Lett.B*, 773:408, 2017.
- [66] C. Loizides et al. *Phys.Rev.C*, 97:054910, 2018.
- [67] M. Gyulassy J. Xu, A. Buzzatti. *JHEP*, 08:063, 2014.
- [68] M. Djordjevic et al. *Phys.Rev.C*, 99:061902, 2019.
- [69] D. Zigic et al. *Nucl.Phys.A*, 00:1, 2020.
- [70] B.Betz and M.Gyulassy. *arXiv*, 1305.6458[nucl-th], 2013.
- [71] B.Betz and M.Gyulassy. *Phys.Rev.C*, 86:024903, 2012.
- [72] B.Betz and M.Gyulassy. *Phys.Rev.C*, 84:024913, 2011.
- [73] A. Adare et al. (PHENIX Collaboration). *Phys.Rev.Lett.*, 101:232301, 2008.
- [74] B. Abelev et. (ALICE Collaboration). *Eur.Phys.J.*, C74:3108, 2014.
- [75] J.D. Bjorken. *Phys.Rev.D*, 27:140, 1982.
- [76] B. Abelev et al. (ALICE Collaboration). *Phys.Rev.C*, 88:044909, 2013.
- [77] N. Jacazio (ALICE Collaboration). *Nucl.Phys.A*, 967:421, 2017.
- [78] J. Adams et al. (STAR Collaboration). *Phys.Rev.Lett.*, 98:062301, 2007.
- [79] B. Abelev et al. (ALICE Collaboration). *Phys.Rev.Lett.*, 111:222301, 2013.
- [80] D.S. de Albuquerque (ALICE Collaboration). *Quark Matter 2018*, 13-19 May 2018.
- [81] I.C. Arsene et al. (BRAHMS Collaboration). *Phys.Rev.C*, 94:014907, 2016.
- [82] F. Bellini (ALICE Collaboration). *Nucl.Phys.A*, 982:427, 2019.
- [83] A. Adare et al. (STAR Collaboration). *Phys.Rev.C*, 93:024901, 2016.
- [84] A. Seryakov and G. Feofilov. *AIP Conference Proceedings*, 1701:070001, 2016.
- [85] J. Adam et al. (ALICE Collaboration). *Eur.Phys.J.*, C77:33, 2017.
- [86] C. Andres et al. *Eur.Phys.J.*, C76:475, 2016.
- [87] C. Andres et al. *arXiv:1705.01493[nucl-th]*, 2017.
- [88] M. Xie et al. *Eur.Phys.J.*, C79:589, 2019.
- [89] E. Sangaline et al. (STAR Collaboration). *Quark Matter 2012 Conference Proceedings*, 2012.
- [90] D. Sekihata (for the ALICE Collaboration). *Quark Matter 2018*, 13-19 May 2018.
- [91] J. Liao and E. Shuryak. *Phys.Rev.Lett.*, 102:202302, 2009.